

Minimal surfaces: a geometric three dimensional segmentation approach

Vicent Caselles¹, Ron Kimmel², Guillermo Sapiro³, Catalina Sbert⁴

¹ Department of Mathematics and Informatics, University of Illes Balears, E-07071 Palma de Mallorca, Spain; e-mail: dmivca0@ps.uib.es

² LBL UC Berkeley, Mailstop 50A-2152, Berkeley, CA 94720, USA; e-mail: ron@csr.lbl.gov

³ Hewlett-Packard Labs, 1501 Page Mill Road, Palo Alto, CA 94304, USA; e-mail: guille@hpl.hp.com

⁴ Department of Mathematics and Informatics, University of Illes Balears, E-07071 Palma de Mallorca, Spain

Received January 4, 1996 / Revised version received August 2, 1996

Summary. A novel geometric approach for three dimensional object segmentation is presented. The scheme is based on geometric deformable surfaces moving towards the objects to be detected. We show that this model is related to the computation of surfaces of minimal area (local minimal surfaces). The space where these surfaces are computed is induced from the three dimensional image in which the objects are to be detected. The general approach also shows the relation between classical deformable surfaces obtained via energy minimization and geometric ones derived from curvature flows in the surface evolution framework. The scheme is stable, robust, and automatically handles changes in the surface topology during the deformation. Results related to existence, uniqueness, stability, and correctness of the solution to this geometric deformable model are presented as well. Based on an efficient numerical algorithm for surface evolution, we present a number of examples of object detection in real and synthetic images.

Mathematics Subject Classification (1991): 53A10

1. Introduction

One of the basic problems in image analysis is object detection. This can be associated with the problem of boundary detection, where boundary is roughly defined as a curve or surface separating homogeneous regions. “Snakes,” or active contours, were proposed by Kass et al. [26] to solve this problem, and received a great deal of attention from the image analysis community since then. The work was later extended to 3D surfaces. The classical snakes and 3D deformable surfaces approaches, reviewed in the following section, are based on deforming

Correspondence to: G. Sapiro

an initial contour or surface towards the boundary of the object to be detected. The deformation is obtained by trying to minimize a functional designed such that its (local) minima is obtained at the boundary of the object. These active surfaces are examples of the general technique of matching deformable models to image data by means of energy minimization [5, 64]. The energy is basically composed by a term which controls the smoothness of the surface and another one that attracts it to the boundary. This energy model is not capable of changing its topology when direct implementations are performed. The topology of the final surface will be in general as that of the initial one, unless special procedures are implemented for detecting possible splitting and merging points [42, 61]. This may be a problem when an un-known number of objects must be simultaneously detected. This approach is also non intrinsic, i.e., the energy functional depends on the parametrization. See for example [40, 67] for comments on advantages and disadvantages of energy approaches for deforming surfaces, as well as an extended literature on different approaches to deformable models.

Recently, geometric models of deformable contours/surfaces were simultaneously proposed by Caselles et al. [6] and by Malladi et al. [39–41], and are also reviewed in the following section. These models are based on the theory of surface evolution and geometric flows, which has gained a large amount of attention from the image analysis community in the past years [2, 3, 19, 20, 21, 29, 30, 32, 33, 35, 36, 44, 50, 51, 54, 55, 56, 57, 58, 63, 65, 66]. In these models, the curve/surface is propagating (deforming) by an implicit velocity that also contains two terms, one related to the regularity of the deforming shape and the other attracting it to the boundary. The model is given by a geometric flow (PDE), based on mean curvature motion, and not by an energy function. This model allows automatic changes in topology when implemented using the level-sets numerical algorithm [48]. Thereby, several objects can be detected simultaneously, without previous knowledge of their exact number in the scene, and without special tracking procedures.

In [7], we showed the relation between these two approaches for two dimensional object detection (two dimensional curve evolution), proposing what we called *geodesic active contours*. We first proved that, for a particular case, the classical energy approach is equivalent to finding a geodesic curve in a Riemannian space with a metric derived from the image. This means that the boundary we are looking for is the path of minimal distance, measured in the Riemannian metric, that connects two given image points. We then showed that assuming a level set representation of the deforming contour, we can find this geodesic curve via a geometric flow which is very similar to the one obtained in the curve evolution approaches mentioned above. This flow, however, includes a new term that improves those models.¹ The new term allows to track, in an accurate way, boundaries with high variation of their gradient, a task that was impossible with previous curve evolution models. We also showed that the solution of the flow ex-

¹ Although this term appears in similar forms in classical snakes, it was missing in curve evolution models. This term is naturally incorporated by the geodesic formulation

ists in the viscosity framework, and is unique and stable. Therefore, the approach presented in [7] has the following main properties:

1. Connects energy and curve evolution approaches of active contours.
2. Presents the snake problem as a geodesic computation one.
3. Improves existing models as a result of the geodesic formulation.
4. Allows simultaneous detection of interior and exterior boundaries in several objects without special contour tracking procedures.
5. Holds formal existence, uniqueness, and stability results.
6. Stops automatically.

In this paper we extend the results in [7] to three dimensional object detection. The obtained geometric flow is based on geometric deformable surfaces. We show that the desired boundary is given by a “minimal surface” in a space defined by the image. Therefore, segmentation is achieved via the computation of surfaces of “minimal area,” where the area is defined in an image dependent space. The obtained flow has the same advantages over other 3D deformable models as the advantages of the geodesic active contours over previous 2D approaches.

Before proceeding we should point out that the deformable surfaces model derived in this paper is related to a number of previously or simultaneously developed results. As we pointed out before, it is closely related to the works of Terzopoulos and colleagues on energy based deformable surfaces, and the works by Caselles et al. and Malladi et al. [6, 39, 40, 41]. It is of course closely related to [7], where the 2D model was derived. The basic equations in this paper, as well as the corresponding 2D ones in [7], were simultaneously developed in [27, 28, 60]. Similar 3D models are studied in [65, 66] as well. Extensions to [6, 39] are presented also in [63]. The similitude and differences with those approaches will be presented after describing the basic principles of the model.

This paper is organized as follows. In Sect. 2 we briefly review both classical energy based and surface evolution based deformable models. In Sect. 3 we describe the main results on 2D geodesic active contours as presented in [7], which will help us to develop the 3D minimal surface deformable models, presented in Sect. 4. Results concerning existence and uniqueness of the proposed model are given in Sect. 5, and those related to its correctness in Sect. 6. Experimental results are given in Sect. 7 and concluding remarks in Sect. 8.

2. Basic approaches on snakes and deformable shapes

2.1. Energy based snakes

We start with a description of classical energy snakes, first for 2D objects and then for 3D ones.

Let $\mathcal{C}(p) : [0, 1] \rightarrow \mathbb{R}^2$ be a parametrized planar curve, and $I : [0, a] \times [0, b] \rightarrow \mathbb{R}^+$ a given image where we want to detect the objects boundaries. The classical snakes approach [26] associates to the curve \mathcal{C} an energy given by

$$(1) \quad E(\mathcal{C}) = \alpha \int_0^1 |\mathcal{C}'(\tau)|^2 d\tau + \beta \int_0^1 |\mathcal{C}''(\tau)|^2 d\tau - \lambda \int_0^1 |\nabla I(\mathcal{C}(\tau))| d\tau,$$

where α , β , and λ are real positive constants (α and β impose the elasticity and rigidity of the curve). The first two terms basically control the smoothness of the contours to be detected (internal energy),² while the third term is responsible for attracting the contour towards the object in the image (external energy). Solving the problem of snakes amounts to finding, for a given set of constants α , β , and λ , the curve \mathcal{C} that minimizes E . As argued in Caselles et al. [6], the snake method provides an accurate location of the edges near a given initialization of the curve and it is capable to extract smooth shapes. They also showed that the snakes model can retrieve angles for all values of parameters $\alpha, \beta \geq 0$ ($\alpha + \beta > 0$). This is, in some sense, related to the adaptation of the set of parameters α, β to the problem in hand. On the other hand, it does not directly allows simultaneous treatment of several contours. Note that when considering more than one object in the image, and for example the initial prediction of \mathcal{C} surrounds all of them, it is not possible to detect all the objects. In other words, the classical (energy) approach of the snakes can not deal with changes in topology, unless special topology handling procedures are added [42]. The topology of the initial curve will be the same as the one of the (possible wrong) final solution. The geometric models in [6, 7, 39, 40, 41, 27, 63, 65] automatically overcome this problem.

It is clear that the classical snake method can be generalized to 3D data images, where the boundaries of the objects are surfaces. This extension is known as the deformable surface model, and was introduced by Terzopoulos et al. [64] for a 3D representation of objects and extended and used for a 3D segmentation by many others (see for example [11, 12, 13]). In the 3D case, a parametrized surface

$$v(r, s) = (x(r, s), y(r, s), z(r, s)) \quad (r, s) \in [0, 1] \times [0, 1]$$

is considered, and the energy functional is given by

$$(2) \quad E(v) = \int_{\Omega} \left[\omega_{10} \left| \frac{\partial v}{\partial r} \right|^2 + \omega_{01} \left| \frac{\partial v}{\partial s} \right|^2 + 2\omega_{11} \left| \frac{\partial^2 v}{\partial r \partial s} \right|^2 + \omega_{20} \left| \frac{\partial^2 v}{\partial r^2} \right|^2 + \omega_{02} \left| \frac{\partial^2 v}{\partial s^2} \right|^2 + P(v(r, s)) \right] dr ds,$$

where $P := -\|\nabla I\|^2$, or any related decreasing function of the gradient. Like the 2D case, the algorithm starts with an initial surface \mathcal{S}_0 , generally near the desired 3D boundary \mathcal{O} , and tries to move \mathcal{S}_0 towards a local minimum of E .

These are the basic formulations of the 2D and 3D snakes. Other related formulations have been proposed in the literature. Reviewing all of them is out of the scope of this paper.

² Other smoothing constraints can be used, being this the most common one

2.2. Deformable models based on mean curvature motion

Recently, novel geometric models of deformable curves were simultaneously proposed by Caselles et al. [6] and by Malladi et al. [39, 40, 41]. Assume in the 2D case that the deforming curve \mathcal{C} is given as a level-set of a function $u : \mathbb{R}^2 \rightarrow \mathbb{R}$. Then, we can represent the deformation of \mathcal{C} via the deformation of u . In this case, the proposed 2D deformation is given by

$$(3) \quad \frac{\partial u}{\partial t} = g(I)|\nabla u| \operatorname{div} \left(\frac{\nabla u}{|\nabla u|} \right) + \nu g(I)|\nabla u| \quad (t, x) \in [0, \infty) \times \mathbb{R}^2$$

$$(4) \quad u(0, x) = u_0(x) \quad x \in \mathbb{R}^2$$

where ν is a positive real constant, $g(I)$ is given by

$$(5) \quad g(I) := \frac{1}{1 + |\nabla \hat{I}|^p},$$

\hat{I} is a regularized version of the original image I where we are looking for the contour of an object O , and $p = 1$ or 2 . Typically, the initial condition $u(0, x) = u_0(x)$, in the case of outer snakes (curves evolving towards the boundary of O from the exterior of O), was taken as a regularized version of $1 - \chi_{\mathcal{C}}$ where $\chi_{\mathcal{C}}$ is the characteristic function of a set \mathcal{C} containing O . Using the fact that

$$\operatorname{div} \left(\frac{\nabla u}{|\nabla u|} \right) = \kappa,$$

where κ is the Euclidean curvature [25] of the level sets \mathcal{C} of u , Equation (3) can be written in the form

$$u_t = g(I)(\nu + \kappa)|\nabla u|.$$

Equation (3) can be interpreted as follows: Suppose that we are interested in following a certain level set of u , which, to fix ideas, we suppose to be the zero level set. Suppose also that this level set is a smooth curve. Then the flow

$$u_t = (\nu + \kappa)|\nabla u|,$$

means that the level set \mathcal{C} of u we are considering is evolving according to

$$(6) \quad \mathcal{C}_t = (\nu + \kappa)\mathcal{N},$$

where \mathcal{N} is the inward normal to the curve.³ This equation was first proposed in [48, 62], where extensive numerical research on it was performed. It was introduced in computer vision in [29, 30] for shape analysis. The motion

$$\mathcal{C}_t = \kappa\mathcal{N},$$

³ Based on the fact that $\mathcal{N} \parallel \nabla u$, and under certain smoothness constraints, it is straightforward to prove that when the level sets \mathcal{C} of u evolve according to $\mathcal{C}_t = \beta\mathcal{N}$, the function u deforms via $u_t = \beta|\nabla u|$

denoted as *Euclidean heat flow* is very well known for its excellent geometric smoothing properties [4, 23, 24]. (This flow was extended in [55, 56, 57] for the affine group and in [19, 46, 57] for others.) This flow is also called the *Euclidean shortening flow*, since it moves the curve in the gradient direction of the length functional given by

$$(7) \quad L := \oint_C ds,$$

where $ds = |C_p|dp$ is the Euclidean arc-length element. Therefore, this flow decreases the length of the curve as fast as possible. This property is important for the geometric interpretation of the geodesic and minimal surface models that are developed in this paper.

The constant velocity $\nu\mathcal{N}$ in (6), which is related with classical mathematical morphology [30, 54] and shape offsetting in CAD [31], acts as the balloon force in [12]. Actually this velocity pushes the curve inwards and it is crucial in the model in order to allow convex initial curves to become non-convex, and thereby detect non-convex objects.⁴ Of course, the ν parameter must be specified a priori in order to make the object detection algorithm automatic. This is not a trivial issue, as pointed out in [6], where possible ways of estimating this parameter are considered. In [6] the authors also present existence and uniqueness results (in the viscosity framework) of the solutions of (3). Recapping, the “force” $(\nu + \kappa)$ acts as the internal force in the classical energy based snakes model. The external force is given by $g(I)$, which is supposed to prevent the propagating curve from penetrating into the objects in the image. In [6, 39, 40, 41], the authors choose $g(I)$ given by (5). \hat{I} was smoothed using Gaussian filtering, but more effective geometric smoothers can be used as well. Note that other decreasing functions of the gradient may be selected as well. For an ideal edge, $\nabla\hat{I} = \delta$, $g = 0$, and the curve stops at the edge ($u_t = 0$). The boundary is then given by the set $u = 0$.

The curve evolution model given by (3) automatically handles different topologies. That is, there is no need to know a priori the topology of the solution. This allows to detect any number of objects in the image, without knowing their exact number. This is achieved with the help of an efficient numerical algorithm for curve evolution, developed by Osher and Sethian [48, 62], and used by others for different image analysis problems [10, 30, 32, 35, 36, 54, 56, 58, 63, 65], and analyzed for example in [9, 18]. In this case, the topology changes are automatically handled, without the necessity for specific monitoring the topology of the deforming curve.

The model (3) can easily be extended to 3D object detection. Let us consider for each $t \geq 0$ a 3D function $u(t, \cdot) : \mathbb{R}^3 \rightarrow \mathbb{R}$, and denote by \mathcal{S} its level-sets (3D surfaces). Then the 3D geometric deformable model is given by:

$$(8) \quad \begin{aligned} \frac{\partial u}{\partial t} &= g(I)|\nabla u| \operatorname{div} \left(\frac{\nabla u}{|\nabla u|} \right) + \nu g(I)|\nabla u| \\ &= g(I)(\nu + \mathbf{H})|\nabla u|, \end{aligned}$$

⁴ A convex curve remains convex when evolving according to the Euclidean heat flow [23].

where now \mathbf{H} is the sum of the two principal curvatures of the level sets \mathcal{S} , that is, twice its mean curvature. This model has the same concepts as the 2D one, and is composed by three elements:

1. A smoothing term. In the case of (8), this smoothing term \mathbf{H} is twice the mean curvature, but other more efficient smoothing velocities as those proposed in [2, 8, 47] can be used.⁵
2. A constant balloon-type force ($\nu|\nabla u|$).
3. A stopping factor ($g(I)$). This is a function of the gradient or other 3D edge detectors [68].

The goal of this paper is to extend this model, motivated by the extension of (3) to the geodesic active contours as was done in [7] and reviewed in the next section.

3. Geodesic active contours

We now review the main results of [7]. Let us consider a particular case of (1), where $\beta = 0$. Two main reasons motivate this selection: First, this will allow us to derive the relation between energy based active contours and geometric curve evolution ones. Second, although having $\beta \neq 0$ adds flexibility and other properties, the regularization effect on the geodesic active contours comes from curvature based curve flows, obtained only from the other terms in (1). This allows to achieve smooth curves in the proposed approach without having the high order derivatives given by $\beta \neq 0$. The use of the curvature driven curve motions for smoothing was proved to be very efficient in previous works [2, 6, 30, 40, 51, 56], and is also supported by our experiments in [7] and Sect. 7. Therefore, curve smoothing will be obtained also with $\beta = 0$, keeping only the first regularization term. Assuming this, and replacing the edge detector $|\nabla I|$ by a general function $g(|\nabla I|)^2$ of the gradient such that $g(r) \rightarrow 0$ as $r \rightarrow \infty$, we obtain,

$$(9) \quad E(\mathcal{C}) = \alpha \int_0^1 |C'(\tau)|^2 d\tau + \lambda \int_0^1 g(|\nabla I(\mathcal{C}(\tau))|)^2 d\tau = E_{\text{int}}(\mathcal{C}) + E_{\text{ext}}(\mathcal{C}).$$

(In order to simplify the notation, we will sometimes write $g(I)$, $g(\mathcal{X})$, or $g(x)$ ($\mathcal{X}, x \in \mathbb{R}^2$ and later $\mathcal{X}, x \in \mathbb{R}^3$) instead of $g(|\nabla I|$.) The goal now is to minimize E in (9) for \mathcal{C} in a certain allowed space of curves. Of course, in (9), only the ratio λ/α counts.

As argued in [7], the functional (9) is not intrinsic, i.e., it depends on the parametrization of the curve. This could be considered as an undesirable property since parametrizations are not related to the geometry of the curve (or object boundary), but only to the velocity they are traveled. Motivated by the discussion

⁵ Although curvature flows smooth curves in 2D [23, 24, 55, 56], no curvature flow that smoothes all possible surfaces (while preserving the topology) was yet found in 3D [47]. Frequently used flows are mean curvature or positive part of Gaussian curvature flows [2, 8].

on ideal edges in [7], we proposed to fix this degree of freedom by fixing the energy level $E_0 = 0$ at the local minima (other values are analyzed in [7] as well). Then with the help of Maupertuis' and Fermat Principles [17], we proved that the solution of (9) is given by a geodesic curve in a Riemannian space. The metric in this Riemannian space is defined by $g_{ij} dx_i dx_j$ with $g_{ij} = g(I)^2 \delta_{ij}$. This means that the object is detected when a curve of minimal length is found. In other words, we proved that minimizing (9) is equivalent to solving

$$(10) \quad \min_{\mathcal{C}} \int_0^1 g(|\nabla I(\mathcal{C}(\tau))|) |\mathcal{C}'(\tau)| d\tau.$$

We have transformed the problem into a problem of geodesic computation in a Riemannian space, according to a new metric (length measure) given by

$$(11) \quad L_R := \int_0^1 g(|\nabla I(\mathcal{C}(\tau))|) |\mathcal{C}'(\tau)| d\tau.$$

Since $|\mathcal{C}'(\tau)| d\tau = ds$, we may write

$$L_R := \int_0^L g(|\nabla I(\mathcal{C}(\tau))|) ds.$$

where L denotes the Euclidean length of $\mathcal{C}(\tau)$. Comparing this with the classical Euclidean length as given in the previous section by (7), we find that the new length is obtained by weighting ds with $g(|\nabla I(\mathcal{C}(\tau))|)$, which contains information regarding the boundary of the object. Therefore, when trying to detect an object, we are not just interested in finding the path of minimal classical length ($\int ds$) but the one which minimizes a new definition of the length which takes into account image characteristics. Note that (10) is general, no assumptions on g were made, besides being a decreasing function. For example, g can be derived from edge-type maps as those in [37]. Therefore, the theory of detection based on geodesic computations given above, and fully described in [7], is general.

In order to find this geodesic curve, we use the steepest descent method which will give us a local minima of (11). Then, the flow minimizing L_R is given by [7]

$$(12) \quad \mathcal{C}_t = (g\kappa - \nabla g \cdot \mathcal{N})\mathcal{N}.$$

To introduce the level set formulation, let us assume that a curve \mathcal{C} is parametrized as a level set of a function $u : [0, a] \times [0, b] \rightarrow \mathbb{R}$. That is, \mathcal{C} is such that it coincides with the set of points in u such that $u = \text{constant}$. (In our case we choose the curve to be represented by the zero level set $u = 0$.) In particular given an initial curve \mathcal{C}_0 we parametrize it as a zero level set of a function u_0 . Then, the level set formulation of the steepest descent method says that solving the above geodesic problem starting from \mathcal{C}_0 amounts to searching for the steady state ($\frac{\partial u}{\partial t} = 0$) of the following evolution equation:

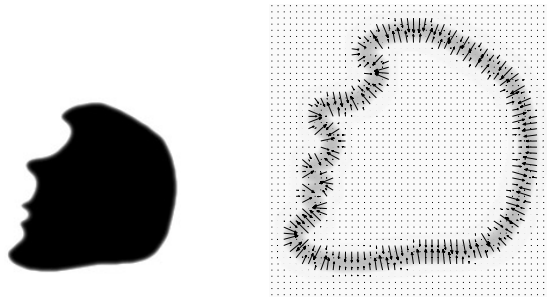


Fig. 1. Geometric interpretation of the new term in the proposed deformable model. The gradient vectors are all directed towards the middle of the boundary. Those vectors direct the propagating curve into the valley of the g function

$$(13) \quad \frac{\partial u}{\partial t} = |\nabla u| \operatorname{div} \left(g(I) \frac{\nabla u}{|\nabla u|} \right)$$

$$(14) \quad = g(I) |\nabla u| \operatorname{div} \left(\frac{\nabla u}{|\nabla u|} \right) + \nabla g(I) \cdot \nabla u,$$

with initial datum $u(0, x) = u_0(x)$. This equation is then obtained by computing the gradient descent of L_R and embedding the flow as the level set of u . We have obtained the main part of the novel active contour model we propose.

Comparing Equation (13) to (3), we see that the term $\nabla g \cdot \nabla u$ is missing in the old model. This is due the fact that in (3), a classical length in Euclidean space is used (given by (7)). In the new model, the length takes into account the image structure, and is given by (11), defining a new Riemannian space. This new term directs the curve towards the boundary of the objects ($-\nabla g$ points toward the center of the boundary). Observe the $2D$ case of an image I of an object of high intensity value and low intensity background. Figure 1 shows a smoothed version of I (left). The function g is shown on the right, together with its gradient vectors. Observe the way the gradient vectors are all directed towards the middle of the boundary. Those vectors direct the propagating curve into the valley of the g function. In this $2D$ case, $\nabla g \cdot \mathcal{N}$ is effective in case the gradient vectors coincide with normal direction of the propagating curve. Otherwise, it will lead the propagating curve into the boundary and eventually force it to stay there. Recapping, this new force increases the attraction of the deforming contour towards the boundary, being of special help when the boundary has high variations of its gradient values. Note that in the old model, the curve stops when $g = 0$. This happens only along an ideal edge. Also, if there are different gradient values along the edge, as it often happens in real images, then g gets different values at different locations along the object boundaries. It is necessary to consider all those values as high enough to guarantee the stopping of the propagating curve. This makes the geometric model (3) inappropriate for the detection of boundaries with (un-known) high variations of the boundary gradients. In our new model, the curve is attracted to the boundary also by the

new term (note again that the gradient vectors point towards the middle of the boundary, Fig. 1). Thereby, it is also possible to detect boundaries with high differences in their gradient values. Another advantage of this new term is that it reduces the importance of the constant velocity given by ν . This constant velocity, that mainly allows the detection of non-convex objects, introduces an extra parameter to the model, that in most cases is an undesirable property. In our case, the new term allows the detection of non-convex objects as well. This term also helps when starting from curves inside the object. In case we wish to add this constant velocity, we can just consider the term $\nu g(I)|\nabla u|$ as an extra speed (which minimizes the enclosed area [12, 67]), in the geodesic problem (10) obtaining

$$(15) \quad \frac{\partial u}{\partial t} = |\nabla u| \operatorname{div} \left(g(I) \frac{\nabla u}{|\nabla u|} \right) + \nu g(I) |\nabla u|.$$

This equation is of course equivalent to

$$(16) \quad \frac{\partial u}{\partial t} = g(\nu + \kappa) |\nabla u| + \nabla u \cdot \nabla g.$$

Equation (15), which is the solution of the geodesic problem (10) with an extra speed, constitutes the *geodesic active contour* model we propose. As shown in the examples in [7], it is possible to choose $\nu = 0$ (no constant velocity), and the model still converges to the correct solution (in a slower motion). The advantage is that we have obtained a model with less parameters.

This equation, as well as its 3D extension (see next section), was recently independently proposed by Kichenassamy et al. [27] based on a slightly different initial approach (being the final form of (10) and (15) identical). Shah [60] also recently presented an active contours formulation as the one in (10). In his case, g is obtained from an elaborated segmentation procedure obtained from the Mumford-Shah approach [43]. Although the works in [27, 60] also present the problem of active contours as geodesic computations, they do not show the connections between energy models and curve evolution ones. Actually, to the best of our knowledge, non of the previous works on curve/surface evolution for object segmentation show the mathematical relation between those models and classical energy approaches, as done in [7] for the 2D case and partially in this paper (next section) for the 3D one. Actually, in general the two approaches are considered independent. In [7] and here we show that they are mathematically connected, and one can enjoy the advantages of both of them in the same model. Although, as we will see in the next section, extension from the 2D model to the 3D one is easy, no 3D examples are presented in [27, 60]. Also, not all the theoretical results here presented can be found in [27, 60]. Three dimensional examples are given in [65], where similar equations as the presented in the next section are proposed. The equations there are obtained by extending the flows in [6, 39], again without showing that they are mathematically related to the classical energy based snakes. In [63], the authors extend the models in [6, 39], motivated by work reported in [29, 30]. One of the key ideas, motivated by the shape theory of shocks developed by Kimia et al., is to perform multiple

initializations, while using the same equations as in [6, 39]. Possible advantages of this are reported in the mentioned manuscript. That paper ([63]) uses the same equations as in [6, 39] and not the new ones described in this paper, also without showing its connection with classical snakes, in contrast with the approach in [7] and here. A normalized version of (10) was derived in [22] from a different point of view, giving as well different flows for 2D active contours. No extension to 3D is presented in that paper.

Existence, uniqueness and stability results for the geodesic active contour model, Equation (15), were stated in [7]. Existence results can also be found in [28]. Analogous results will be stated below (see Sect. 5) for the corresponding 3D extension which we introduce in the next section. We also present consistency results for our 3D model.

4. Three dimensional deformable models as minimal surfaces

In the previous section, we presented a model for 2D object detection based on the computation of geodesics in a given Riemannian space. This means that we are computing paths or curves of minimal (weighted) length. This extends to 3D surfaces by computing surfaces of “minimal area,” where area is defined in an image dependent space. In the 2D case, length is given by (7), and the new length which allows to perform object detection is given by (11). In the case of surfaces, (7) is replaced by area

$$(17) \quad A := \int \int da,$$

and (11) by “weighted” area

$$(18) \quad A_R := \int \int g(I)da,$$

where da is the (Euclidean) element of area. The weighted area A_R is a natural 3D extension to the weighted 2D arc-length L_R , and is thereby the natural analog to the non intrinsic energy minimization (2). Surfaces minimizing (17) are denoted as *minimal surfaces* [49]. In the same way, we will denote by minimal surfaces these surfaces that minimize (18). The difference between A and A_R is like the difference between L and L_R . In A , the element of area is given by the classical element da in Euclidean space, while in A_R , the “area element” da_r is given by $g(I)da$. The basic element of our deformable model will be given by minimizing (18) by means of an evolution equation obtained from its Euler-Lagrange. Given the definition of A_R above, the computations are straightforward and are direct extension of the geodesic active contours computation as presented in the previous section and in [7]. We will point out only the basic characteristics of this flow.

The Euler-Lagrange of A is given by the mean curvature \mathbf{H} , obtaining a curvature flow

$$(19) \quad \frac{\partial \mathcal{S}}{\partial t} = \mathbf{H}\mathcal{N},$$

where \mathcal{S} is the 3D surface and \mathcal{N} its inner unit normal. In a level sets notation, if for each $t \geq 0$, the evolving surface \mathcal{S} is the zero level set of a function $u(t, \cdot) : \mathbb{R}^3 \rightarrow \mathbb{R}$, which we take negative inside \mathcal{S} and positive outside, we obtain the equation

$$(20) \quad u_t = |\nabla u| \operatorname{div} \left(\frac{\nabla u}{|\nabla u|} \right) = |\nabla u| \mathbf{H}.$$

Therefore, the mean curvature motion provides a flow that computes (local) minimal surfaces [10].

Computing now the Euler-Lagrange of $A_{\mathbf{R}}$, we get

$$(21) \quad \mathcal{S}_t = (g\mathbf{H} - \nabla g \cdot \mathcal{N})\mathcal{N}.$$

This is the basic weighted minimal surface flow. Taking a level set representation, in analogy with (13), the steepest descent method to minimize (18) gives

$$(22) \quad \begin{aligned} \frac{\partial u}{\partial t} &= |\nabla u| \operatorname{div} \left(g(I) \frac{\nabla u}{|\nabla u|} \right) \\ &= g(I) |\nabla u| \operatorname{div} \left(\frac{\nabla u}{|\nabla u|} \right) + \nabla g(I) \cdot \nabla u. \end{aligned}$$

However, now u is a 4D function with \mathcal{S} its 3D zero level set. We note again that comparing with previous surface evolution approaches for 3D object detection, the minimal surfaces model includes a new term, $\nabla g \cdot \nabla u$.

As in the 2D case, we can add a constant force to the minimization problem (it is easy to show that this force minimizes the enclosed weighted volume $\int g dx dy dz$), obtaining the general *minimal surfaces model* for object detection:

$$(23) \quad \frac{\partial u}{\partial t} = |\nabla u| \operatorname{div} \left(g(I) \frac{\nabla u}{|\nabla u|} \right) + \nu g(I) |\nabla u|.$$

This is the flow we will further analyze and use for 3D object detection. It has the same properties and geometric characteristics as the geodesic active contours, leading to accurate numerical implementations and topology free object segmentation.

4.1. Estimation of the constant velocity ν

One of the critical issues of the model presented above is to estimate ν (see next section for the related theoretical results). We present now a possible way of doing this. (Another technique for estimating ν can be obtained from the results in [67].)

In [14] it was shown that the maximum curvature magnitude along the geodesics minimizing L_R is given by

$$\max\{|\kappa|\} = \sup_{\tau \in [0,1]} \left\{ \frac{|\nabla g(\mathcal{C}(\tau)) \cdot \mathcal{N}|}{g(\mathcal{C}(\tau))} \right\}.$$

This result is obtained directly from the Euler-Lagrange equation of (11). It leads to an upper bound over the maximum curvature magnitude along the geodesics, given by

$$|\kappa| \leq \sup_{p \in [0,a] \times [0,b]} \left\{ \frac{|\nabla g(I(p))|}{g(I(p))} \right\},$$

which does not require the geodesic itself for limiting the curvature values. In [14] this bound helped in the construction of different potential functions.

A straightforward generalization of this result to our three dimensional model yields the bound over the mean curvature \mathbf{H} . From the equations above, it is clear that for a steady state (*i.e.* $\mathcal{S}_t = 0$) the mean curvature along the surface \mathcal{S} is given by

$$\mathbf{H} = \frac{\nabla g \cdot \mathcal{N}}{g} - \nu.$$

We readily obtain the following upper bound for the mean curvature magnitude along the final surface

$$|\mathbf{H}| \leq \sup \left\{ \frac{|\nabla g|}{g} \right\} + |\nu|,$$

where the sup operation is taken over all the 3D domain. The above bound gives an estimation of the allowed gaps in the edges of the object to be detected as a function of ν . A pure gap is defined as a part of the object boundary at which, for some reason, $g = \text{constant} \neq 0$ at a large enough neighborhood. At these locations $|\mathbf{H}| = |\nu|$. Therefore, pure gaps of radius larger than $1/\nu$ will cause the propagating surface to penetrate into the segmented object. It is also clear that $\nu = 0$, allows the detection of gaps of any given size, and the boundary at such places will be detected as the minimal surface ‘gluing’ the gaps’ boundaries.

5. Existence and uniqueness results for the minimal surfaces model

As shown in the previous section, our 3D object detection model is given by

$$(24) \quad u_t = g(I)|\nabla u| \left(\operatorname{div} \left(\frac{\nabla u}{|\nabla u|} \right) + \nu \right) + \nabla g \cdot \nabla u \quad (t, x) \in [0, \infty) \times \mathbb{R}^3,$$

with initial condition $u(0, x) = u_0(x)$, and⁶

$$g(I) = \frac{1}{1 + |\nabla G_\sigma * I|^2}$$

⁶ A specific g function is selected for the analysis, while as explained before, the model is general

with $\nu > 0$ representing a constant force in the normal direction to the level sets of u , I is the original image where we are looking for the boundary of an object O , $G_\sigma * I$ is the regularized version of it by convolution with a Gaussian G_σ of variance σ .⁷ $u_0(x)$ is the initial condition, usually taken as a regularized version of $1 - \chi_C$ where χ_C is the characteristic function of a set C containing O , in the case of outer deforming models (surfaces evolving towards the objects' boundary ∂O from the exterior of O), or a regularized version of χ_C where C is a set in the interior of O in the case of inner deforming models (surfaces evolving towards ∂O , starting from the inner side of O). Although only 2D outer snakes were considered in [6], we also consider the inner snakes since it seems natural for some applications [7].

Model (24) should be solved in $R = [0, 1]^3$ with Neumann boundary conditions. To simplify the presentation, and as is usually done in the literature we extend the images by reflection to \mathbb{R}^3 and we look for solutions of (24) which are periodic, i.e., satisfying $u(t, x + 2h) = u(t, x)$ for all $x \in \mathbb{R}^3$ and $h \in \mathbb{Z}$. The initial condition $u_0(x)$ and $g(x)$ are extended to \mathbb{R}^3 with the same periodicity as u .

Existence and uniqueness results for equation (24) can be proved using the theory of viscosity solutions [15]. First we rewrite equation (24) in the form

$$(25) \quad \frac{\partial u}{\partial t} - g(x)a_{ij}(\nabla u)\partial_{ij}u - \nu g(x)|\nabla u| - \nabla g \cdot \nabla u = 0 \quad (t, x) \in [0, \infty) \times \mathbb{R}^3,$$

where $a_{ij}(p) = \delta_{ij} - \frac{p_i p_j}{|p|^2}$ if $p \neq 0$. We use the usual notations $\partial_i u = \frac{\partial u}{\partial x_i}$, $\partial_{ij} u = \frac{\partial^2 u}{\partial x_i \partial x_j}$ and the classical Einstein summation convention in (25) and in all what follows.

Let us recall the definition of viscosity solutions. Let $u \in C([0, T] \times \mathbb{R}^3)$ for some $T \in (0, \infty)$. We say that u is a viscosity subsolution of (24) if for any function $\phi \in C^2(\mathbb{R} \times \mathbb{R}^3)$ and any local maximum $(t_0, x_0) \in (0, T] \times \mathbb{R}^3$ of $u - \phi$ we have: if $\nabla \phi(t_0, x_0) \neq 0$, then

$$\begin{aligned} \frac{\partial \phi}{\partial t}(t_0, x_0) - g(x_0)a_{ij}(\nabla \phi(t_0, x_0))\partial_{ij} \phi(t_0, x_0) \\ - \nu g(x_0)|\nabla \phi(t_0, x_0)| - \nabla g(x_0) \cdot \nabla \phi(t_0, x_0) \leq 0 \end{aligned}$$

and if $\nabla \phi(t_0, x_0) = 0$, then

$$\frac{\partial \phi}{\partial t}(t_0, x_0) - g(x_0) \limsup_{p \rightarrow 0} a_{ij}(p)\partial_{ij} \phi(t_0, x_0) \leq 0$$

and $u(0, x) \leq u_0(x)$ for all $x \in \mathbb{R}^3$. In the same way we define the notion of viscosity supersolution changing "local maximum" by "local minimum", " ≤ 0 " by " ≥ 0 " and "lim sup" by "lim inf" in the expressions above. A viscosity solution is a function which is a viscosity subsolution and a viscosity supersolution.

The existence result in [6, 7] can be easily adapted to the 3D case and we recall them without proof.

⁷ Once again, the Gaussian is just an example of smoothing operator used for the analysis

Theorem 1. Let $W^{1,\infty}$ denote the space of bounded Lipschitz functions in \mathbb{R}^3 . Assume that $g \geq 0$ is such that $\sup\{|\nabla g^{\frac{1}{2}}(x)| : x \in \mathbb{R}^3\} < \infty$ and $\sup\{|\partial_{ij}g(x)| : x \in \mathbb{R}^3, i, j = \{1, 2, 3\}\} < \infty$. Let $u_0, v_0 \in C(\mathbb{R}^3) \cap W^{1,\infty}(\mathbb{R}^3)$. Then

1. Equation (24) admits a unique viscosity solution $u \in C([0, \infty) \times \mathbb{R}^3) \cap L^\infty(0, T; W^{1,\infty}(\mathbb{R}^3))$ for all $T < \infty$. Moreover, it satisfies

$$\inf_{\mathbb{R}^3} u_0 \leq u(t, x) \leq \sup_{\mathbb{R}^3} u_0.$$

2. Let $v \in C([0, \infty) \times \mathbb{R}^3)$ be the viscosity solution of (24) with initial data v_0 . Then for all $T \in [0, \infty)$ we have

$$\sup_{0 \leq t \leq T} \|u(t, x) - v(t, x)\|_{L^\infty(\mathbb{R}^3)} \leq \|u_0(x) - v_0(x)\|_{L^\infty(\mathbb{R}^3)},$$

which means that the solution is stable.

The assumptions of Theorem 1 are just technical. They imply the smoothness of the coefficients of (25) required to prove the result using the method in [3], [6]. In particular, Lipschitz continuity in x is required. This implies a well defined trajectory of the flow $X_t = \nabla g(X)$, passing through any point $X_0 \in \mathbb{R}^3$, which is a reasonable assumption in our context. The proof of this theorem follows the same steps of the corresponding proofs for the model (3) (see [6], Theorem 3.1), and we shall omit the details (see also [3]).

In the next Theorem, we recall a result on the independence of the generalized evolution with respect to the embedding function u_0 .

Theorem 2. Let $u_0 \in W^{1,\infty}(\mathbb{R}^3) \cap BUC(\mathbb{R}^3)$. Let $u(t, x)$ be the solution of Equation (25) as in Theorem 1. Let $\Gamma_t := \{x : u(t, x) = 0\}$ and $D_t := \{x : u(t, x) \geq 0\}$. Then (Γ_t, D_t) are uniquely determined by (Γ_0, D_0) .

This theorem is adapted from [9], where a slightly different formulation is given. The techniques there can be applied to the present model.

Let us present some further remarks on the proposed flows (22), (23), as well as the previous geometric model (3). First note that these equations are invariant under increasing re-arrangements of contrast (morphology invariance [2]). This means that $\Theta(u)$ is a viscosity solution of the flow if u and $\Theta : \mathbb{R} \rightarrow \mathbb{R}$ are increasing functions. On the other hand, while (22) is also contrast invariant, i.e., invariant to the transformation $u \leftarrow -u$, Equations (3) and (23) are not, due to the presence of the constant velocity term $\nu g(I)|\nabla u|$. This has a double effect. First, for Equation (22), it can be shown that the generalized evolution of the level sets Γ_t only depends on Γ_0 ([18], Theorem 2.8), while for (23), the result in Theorem 2 is given. Second, for Equation (22) one can show that if a smooth classical solution of the weighted minimal surface flow with $\nu = 0$ exists and is unique, then it coincides with the generalized solution obtained via the level-sets representation (22) during the lifetime of existence of the classical solution ([18], Theorem 6.1). The same result can then be proved for the general

minimal surface flow ($\nu \neq 0$) and its level set representation (23), although a more delicate proof, on the lines of Corollary 11.2 in [59], is required.

The next general result, see also Lemma 2 below, will be needed in the following section to study the asymptotic behavior of the minimal surfaces model (24). Since the proof is an easy adaptation of the one in [9] (Theorem 3.2), we shall omit it as well.

Lemma 1. *Assume $S = \{x \in [0, 1]^3 : g(x) = 0\}$ is a smooth compact surface, $g \geq 0$ and $\nabla g(x) = 0$ for all $x \in S$, and assume that $u_0(x) \in W^{1,\infty}(\mathbb{R}^3)$ is periodic with fundamental domain $[0, 1]^3$, vanishing in an open neighborhood of S . Let $u(t, x)$ be the viscosity solution of the minimal surfaces flow. Then*

$$u(t, x) = 0 \quad \forall x \in S, \quad \forall t \geq 0.$$

6. Correctness of the geometric minimal surfaces model

By correctness we mean the consistency of the results with our initial purpose of object detection, in an ideal case. A smooth surface in an ideal image with no noise should be recovered by our model. In this section we deal with this point.

To study the asymptotic behavior of the equation

$$(26) \quad u_t = g(x)|\nabla u| \left(\operatorname{div} \left(\frac{\nabla u}{|\nabla u|} \right) + \nu \right) + \nabla g \cdot \nabla u \quad (t, x) \in [0, \infty) \times \mathbb{R}^3$$

with initial condition

$$u(0, x) = u_0(x), \quad \forall x \in \mathbb{R}^3,$$

we assume that $S = \{x \in [0, 1]^3 : g(x) = 0\}$ is a compact surface of class C^2 . S divides the cube $[0, 1]^3$ into two regions: the interior region and the exterior region of S . Denote these regions by $I(S)$ and $E(S)$, respectively. Observe that the interior $I(S)$ may have several connected components and $I(S)$ describes all of them together. The initial datum u_0 will be always taken in $C^2(\mathbb{R}^3)$ periodic with fundamental domain $[0, 1]^3$ and vanishing in an open neighborhood of $S \cup I(S)$. Moreover, we take $u_0(x)$ such that its level sets have uniformly bounded curvatures. Let $u(t, x)$ be the unique viscosity solution of (26) given by Theorem 1 above. We follow the evolution of the set $G(t) = \{x \in [0, 1]^3 : u(t, x) = 0\}$ whose boundary $S(t)$ we are interested in.

Before going into the details let us recall some elementary notions of differential geometry required below. A surface of *genus* p is a surface obtained by removing the interiors of $2p$ disjoint disks from the sphere S^2 and attaching p disjoint cylinders to their boundaries. We define the Euler-Poincaré Characteristic of a surface S as $\chi(S) = 2 - 2p$ where p is its genus. We say that a surface S such that $\chi(S) = 2 - 2p$ is *unknotted* if every diffeomorphism from S to a standard p -torus can be extended to a diffeomorphism of \mathbb{R}^3 .

We can assume that $g \geq 0$, $\forall x \in [0, 1]^3$; and $\nabla g = 0$, $\forall x \in S$. Then, for some function $h \geq 0$ we have $g(x) = h(x)^2$ and the equation (26) in the form

$$(27) \quad u_t = h(x) \left(h(x) |\nabla u| \left(\operatorname{div} \left(\frac{\nabla u}{|\nabla u|} \right) + \nu \right) + 2 \nabla h \cdot \nabla u \right).$$

With this formulation, $S = \{x \in [0, 1]^3 : h(x) = 0\}$.

In this section we are going to prove the following:

Theorem 3. Assume $S = \{x \in [0, 1]^3 : g(x) = 0\}$ is diffeomorphic to a sphere, i.e., $\chi(S) = 2$. If the constant ν is sufficiently large, then $S(t)$ converges to S in the Hausdorff distance as $t \rightarrow \infty$.

Theorem 4. Assume $S = \{x \in [0, 1]^3 : g(x) = 0\}$ is diffeomorphic to a p -torus, i.e., $\chi(S) = 2 - 2p$ and is unknotted. If ν is sufficiently large, then $S(t)$ converges to S in the Hausdorff distance as $t \rightarrow \infty$.

Theorem 5. Assume $S = \{x \in [0, 1]^3 : g(x) = 0\}$ is the knotted surface of Fig. 5. If ν is sufficiently large, then $S(t)$ converges to S in the Hausdorff distance as $t \rightarrow \infty$.

Proof of Theorem 3. The proof is based on Lemma 2 and Lemma 3 below.

Lemma 2. $I(S) \subset \{x \in [0, 1]^3 : u(t, x) = 0\}$ for all $t > 0$

Proof. In Theorem 1 we proved that $u(t, x) = 0$ for all $x \in S$ and all $t > 0$. Consider the problem

$$(28) \quad \begin{aligned} z_t &= g(x) |\nabla z| \left(\operatorname{div} \left(\frac{\nabla z}{|\nabla z|} \right) + \nu \right) + \nabla g \cdot \nabla u & (t, x) \in [0, \infty) \times I(S) \\ z(0, x) &= u_0(x) & x \in I(S) \\ z(t, x) &= 0 & x \in S \quad t \geq 0 \end{aligned}$$

We know that $z(t, x) = 0$ and $z(t, x) = u(t, x)$ are two viscosity solutions of (28). Since there is uniqueness of viscosity solutions of this problem, it follows that $u(t, x) = 0$ for all $(t, x) \in [0, \infty) \times I(S)$. \square

Remark. Lemma 2 is also true if S is as in Theorem 4.

Lemma 3. Assume $S = \{x \in [0, 1]^3 : g(x) = 0\}$ is diffeomorphic to a sphere, i.e., $\chi(S) = 2$. If the constant ν is sufficiently large, for any $\eta > 0$, there exists some $T_\eta > 0$ such that

$$G(t) \subset \{x \in [0, 1]^3 : d(x, I(S)) < 2\eta\}$$

for all $t > T_\eta$.

Proof. Essentially, the proof of this lemma consists in constructing a subsolution of (26) which becomes strictly positive as $t \rightarrow \infty$. If S is a convex C^2 surface this is not a difficult task. In this case the distance function to S , $d(x) = d(x, S)$, $x \in E(S)$ is of class C^2 in $E(S)$. This function is the tool to construct the desired subsolution. In the general case S needs not be convex and the proof is a bit more technical and we need a geometric construction.

Let S_1 be a compact surface of class C^2 contained in $\{x \in [0, 1]^3 : u_0(x) > 0\} \cap E(S)$. Consider $E = \{x \in [0, 1]^3 : x \in I(S_1) \cap E(S)\}$. E is diffeomorphic to the closed annulus $A = \{x \in \mathbb{R}^3 : r' \leq |x| \leq r''\}$. There is a C^2 diffeomorphism ϕ between A and E . Consider the family ζ_r of surfaces

$$\begin{aligned} \zeta_r(\theta, \varphi) &= (r \cos \theta \cos \varphi, r \cos \theta \sin \varphi, r \sin \theta) \\ r' \leq r \leq r'', \quad -\frac{\pi}{2} < \theta \leq \frac{\pi}{2}, \quad 0 \leq \varphi < 2\pi. \end{aligned}$$

This family is mapped by ϕ into a family of surfaces $S(r)$ in E of class C^2 , i.e. $S(r) = \phi \circ \zeta_r$. Without loss of generality we may suppose that $\Gamma(r') = S$ and $\Gamma(r'') = S_1$. Since the surfaces ζ_r , $r' \leq r \leq r''$ have uniformly bounded curvatures it follows that the family of surfaces $S(r)$, $r' \leq r \leq r''$ have uniformly bounded curvatures.

We may choose $\rho > 0$ such that we have $\nabla h \cdot \nabla d(x, S) > 0$ on $E(S) \cap (S + B(0, \rho))$.

For any $\eta > 0$, we can take $n = n(\eta)$ and $r'' = r_1 > r_2 > \dots > r_n$ sufficiently close to each other and r_n near to r' such that the family of surfaces $S_i = \phi \circ \zeta_{r_i}$ satisfies the following:

1. $S_i \in C^2$ with interior region $I(S_i)$ and exterior region $E(S_i)$, $i = 1, \dots, n$, and with $S_i \subset I(S_{i-1})$, $i = 2, \dots, n$.
2. $S_1 \subset \{x \in [0, 1]^3 : u_0(x) > 0\}$ and $S_n \subset \{x \in E(S) : 0 < d(x, S) < \eta\}$.
3. For each $x \in S_i$, let $k_i^j(x)$, $j = 1, 2$ the principal curvatures of S_i at the point x . Let $K_i = \max\{|k_i^j(x)| : x \in S_i, j = 1, 2\}$. We suppose (to ensure regularity) that $S_i \subset \{x \in E(S_{i+1}) : d(x, S_{i+1}) < \frac{1}{2K_{i+1}}\}$.
4. $\sup\{K_i, i = 1, \dots, n\} \leq M$ with a constant M independent of η .

From these surfaces we construct another family S_i^* such that, $S_1^* = S_1$ and for each $i = 2, \dots, n-1$, let S_i^* be a regular surface contained in $\{x \in E(S_i) \cap I(S_{i-1}) : d(x, S_i) < \frac{1}{4K_{i+1}}\}$. Finally, let S_n^* be a smooth surface contained in $\{x \in E(S_n) \cap I(S_{n-1}) : d(x, S) < 2\eta\}$. Each surface S_i^* is in a neighborhood of S_{i+1} of radius $\frac{3}{4K_{i+1}}$.

Let R_i be the region between the surfaces S_{i-1}^* and S_i , $i = 2, \dots, n$ (see Fig. 2). Let $d_i(x) = d(x, S_i)$ for $x \in R_i$, and let $C_i > 0$ be a constant such that $d_i(x) \leq C_i h(x)$ for $x \in R_i$, $i = 2, \dots, n$. Notice also that we are working in the unit cube and $d_i(x) \leq \sqrt{3}$. We may also suppose that there exists $n' < n$ such that for $i \geq n'$ we have $R_i \subset E(S) \cap (S + B(0, \rho))$. Since assuming that $\nabla h \cdot \nabla d(x, S) > 0$, by continuity we may choose ρ small enough such that when $i \geq n'$ we have $\nabla h \cdot \nabla d_i \geq 0$.

Our purpose is to construct a family of subsolutions, which becomes asymptotically positive as $t \rightarrow \infty$ on each R_i . By the last of our assumptions on u_0 , we may choose a constant ν in (27) sufficiently large independent of the geometric construction such that for some $\delta > 0$

$$(29) \quad \Delta d_i + \nu \geq \delta > 0 \quad \text{in } R_i \quad i = 2, \dots, n$$

and u_0 is a subsolution of the (27), i.e.

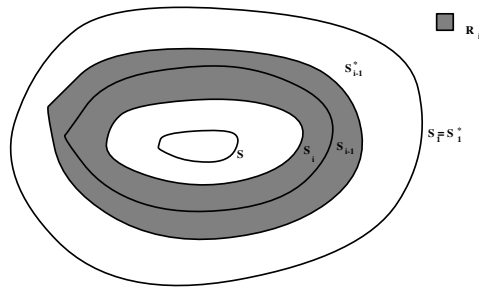


Fig. 2. Construction for Lemma 2

$$(30) \quad |\nabla u_0| h(x) \left(\operatorname{div} \left(\frac{\nabla u_0}{|\nabla u_0|} \right) + \nu \right) + 2\nabla h \cdot \nabla u_0 \geq 0. \square$$

Remark. If $i \leq n' - 1$ we take ν large enough such that $\delta > \frac{2C}{\inf_{E(S) \cap (S+B(0,\rho))} h}$ where C is an upper bound for $|\nabla h \cdot \nabla d_i|$, $i = 2, \dots, n' - 1$. With this we obtain that for some $\delta_1 > 0$,

$$h(x)(\Delta d_i + \nu) + 2\nabla h \cdot \nabla d_i \geq \delta_1 > 0 \quad x \in R_i, \quad i = 2, \dots, n' - 1.$$

If $i \geq n'$ we have $R_i \subset E(S) \cap (S + B(0, \rho))$, and $Dh \cdot \nabla d_i > 0$. In this case, we also obtain that, for some $\delta_2 > 0$,

$$h(x)(\Delta d_i + \nu) + 2\nabla h \cdot \nabla d_i \geq \delta_2 > 0 \quad i \geq n'$$

On each region R_i we consider the problem:

$$(31) \quad \begin{aligned} z_t &= g(x)|\nabla z| \left(\operatorname{div} \left(\frac{\nabla z}{|\nabla z|} \right) + \nu \right) + \nabla g \cdot \nabla z & (t, x) \in [T_{i-1}, \infty) \times R_i \\ z(t, x) &= 0 & x \in S_i \quad t \in [T_{i-1}, \infty) \\ z(t, x) &= u(t, x) & x \in S_{i-1}^* \quad t \in [T_{i-1}, \infty) \\ z(T_{i-1}, x) &= 0 & x \in R_i \end{aligned}$$

where T_i will be specified later. We want to construct a family of subsolutions of (31) which becomes positive as $t \rightarrow \infty$. Obviously $u(t, x)$, the viscosity solution of (26) given by Theorem 1, is a supersolution of the problem (31), and by (30) u_0 is a subsolution of (26). We shall use the following comparison principle [15].

Theorem 6. Let $w, v \in C([0, \infty), C(R_i))$ be respectively a bounded sub and supersolution of (31). Then $w(t, x) \leq v(t, x)$ for all $(t, x) \in [0, \infty) \times R_i$. The same comparison holds for (26).

The previous result implies $u(t, x) \geq u_0(x)$ for all $(t, x) \in [0, \infty) \times \mathbb{R}^3$. In particular we have

$$(32) \quad \inf\{u(t, x) : t \in [0, \infty), x \in E(S_1^*)\} \geq \inf\{u_0(x), x \in E(S_1^*)\} > 0.$$

Assume we have shown that for all $j < i$ there exists some T_j such that

$$(33) \quad \inf\{u(t, x) : t \in [T_j, \infty), x \in E(S_j^*)\} \geq \beta_j > 0.$$

By (32) this is true when $i = 2$ with $T_1 = 0$.

For constructing the subsolution of (31) in $[T_{i-1}, \infty) \times R_i$, $i = 2, \dots, n$ we change variables and take $T_{i-1} = 0$. Let

$$(34) \quad w_m(t, x) = f_m(t)d_i(x) + g_m(t),$$

where $(t, x) \in [0, \infty) \times R_i$, $m > 0$

$$(35) \quad f_m(t) = \lambda \left(1 - \frac{1}{(1+t)^m}\right) \quad \lambda > 0$$

$$(36) \quad g_m(t) = g_m t \quad t \in [0, t_m] \quad g_m(t) = g_m t_m \quad t > t_m,$$

where $g_m = -2m\lambda$ and $t_m = (1 + \frac{mC_i}{\delta_0})^{\frac{1}{m}} - 1$ where $\delta_0 = \min(\delta_1, \delta_2)$. With these functions we have

Lemma 4. For $\lambda > 0$ small enough and for all $m > 0$, w_m is a subsolution of (31).

Proof. It is clear by construction that $w_m(t, x) \leq 0$ for $(t, x) \in [T_{i-1}, \infty) \times S_i$ and $w_m(T_{i-1}, x) \leq 0$ for $x \in R_i$.

Using (33), taking $\lambda > 0$ sufficiently small, we have $w_m(t, x) \leq u(t, x)$ for $(t, x) \in [T_{i-1}, \infty) \times S_{i-1}^*$.

The function w_m has been chosen such that

$$(37) \quad \frac{\partial w_m}{\partial t} - h(x) \left(h(x) |\nabla w_m| \left(\operatorname{div} \left(\frac{\nabla w_m}{|\nabla w_m|} \right) + \nu \right) + 2Dh \cdot \nabla w_m \right) \leq 0 \text{ in } [0, \infty) \times R_i.$$

Indeed, if $t < t_m$ we have

$$\begin{aligned} & f_m'(t)d_i(x) + g_m'(t) - h(x)f_m'(t)(h(x)(\Delta d_i + \nu) + 2\nabla h \cdot \nabla d_i) \\ & \leq f_m'(t)d_i(x) + g_m \leq f_m'(0)d_i(x) + g_m \leq \sqrt{3}\lambda m + g_m \leq q_0. \end{aligned}$$

If $t > t_m$ we have

$$\begin{aligned} & f_m'(t)d_i(x) - h(x)f_m'(t)(h(x)(\Delta d_i + \nu) + 2\nabla h \cdot \nabla d_i) \\ & \leq f_m'(t)C_i h(x) - h(x)f_m'(t)\delta_0 \leq f_m'(t_m)C_i h(x) - h(x)f_m'(t_m)\delta_0. \end{aligned}$$

Using the expressions for t_m we immediately see that the last expression is ≤ 0 . This completes the proof of the lemma. \square

Lemma 5. $u(t, x) \geq w_m(t, x)$ for all $(t, x) \in [T_{i-1}, \infty) \times R_i$. Hence, there exist $m_0 > 0$ and $T_i > 0$ such that

$$u(t, x) \geq \inf\{w_m(t, x) : t \in [T_{i-1}, \infty), x \in R_i \cap E(S_i^*)\} > 0$$

for all $t \in [T_{i-1}, \infty)$, $x \in R_i \cap E(S_i^*)$ and all $m < m_0$.

Proof. The first inequality follows from Lemma 4 and Theorem 6. On the other hand we observe that

$$(38) \quad w_m(t, x) \rightarrow \lambda d_i(x) + g_m t_m \quad \text{as } t \rightarrow \infty.$$

Since t_m is bounded and $g_m \rightarrow 0$ as $m \rightarrow 0$, there exists some $m_0 > 0$ such that

$$(39) \quad \inf\{\lambda d_i(x) + g_m t_m : x \in R_i \cap E(S_i^*)\} > 0$$

for all $0 < m < m_0$. The lemma follows from (38) and (39). \square

Lemma 5 is a consequence of the last two lemmas.

Extension for $\nu = 0$: If we consider the model (27) with $\nu = 0$, i.e.,

$$(40) \quad u_t = g(x)|\nabla u| \operatorname{div} \left(\frac{\nabla u}{|\nabla u|} \right) + \nabla g(x) \cdot \nabla u$$

with $g(x) = h^2(x)$ as above, a theorem similar to Theorem 3 above holds if we take our initial surface sufficiently close to S . For that, we consider (40) on $[0, +\infty) \times V$ where V is a neighborhood of $I(S)$ together with initial and boundary conditions

$$\begin{aligned} u(0, x) &= u_0(x) & x \in V \\ u(t, x) &= u_0(x) & t > 0 \quad x \in \partial V \end{aligned}$$

Moreover, V should be taken sufficiently near to S , i.e., $V \subset I(S) + B(0, \rho)$ for ρ small enough, so that

$$h(x)\Delta d(x) + 2\nabla h(x) \cdot \nabla d(x) \geq 0 \quad x \in V - \overline{I(S)},$$

where $d(x) = d(x, S)$. In that case, we can adapt the ideas above to prove that $S(t) = \partial\{x : u(t, x) = 0\} \rightarrow S$ as $t \rightarrow \infty$. \square

Proof of Theorem 4.

Lemma 6. *Suppose that $S = \{x \in [0, 1]^3 : g(x) = 0\}$ is diffeomorphic to a p -torus, i.e., $\chi(S) = 2 - 2p$ and is unknotted. If ν is sufficiently large, for any $\eta > 0$ there exist some $T_\eta > 0$ such that*

$$G(t) \subset \{x \in [0, 1]^3 : d(x, I(S)) < \eta\} \quad t > T_\eta.$$

Proof. The idea of the proof is to construct two surfaces Γ_1 and Γ_2 of class C^2 and diffeomorphic to a sphere, i.e. $\chi(\Gamma_i) = 2$, $i = 1, 2$, such that the boundary of $I(\Gamma_1) \cap I(\Gamma_2)$ is diffeomorphic to a p -torus and near S . We prove that for a large t , $S(t)$ is near the boundary of $I(\Gamma_1) \cap I(\Gamma_2)$, therefore $S(t)$ will be near S . Let us, first of all, construct the surfaces Γ_1 and Γ_2 .

Given $\eta > 0$ we choose Γ_1 and Γ_2 satisfying:

1. Γ_i is a compact surface of class C^2 , $\chi(\Gamma_i) = 2$ and $I(S) \subset I(\Gamma_i)$ $i = 1, 2$.
2. $U_\eta := [I(\Gamma_1) + B(0, \frac{\eta}{2})] \cap [I(\Gamma_2) + B(0, \frac{\eta}{2})]$ is an open set whose boundary is a regular surface diffeomorphic to a p -torus.

3. $U_\eta \subset I(S) + B(0, \eta)$

Recall that the sum of two sets A, B is defined by $A+B = \{a+b : a \in A, b \in B\}$

If S is a standard p -torus, which we denote by T_p , it is easy to construct surfaces I_1 and I_2 satisfying the conditions above. Since this is technically delicate, but easy to see graphically, we illustrate it in Fig. 3.

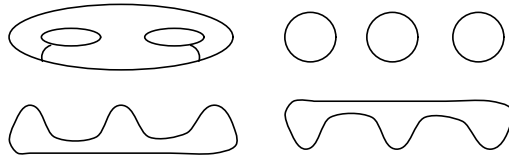


Fig. 3. Construction of I_1 and I_2 for Lemma 5

If S is not a standard p -torus, then (see [16], Chap. 4) it is diffeomorphic to a standard p -torus and there exists a diffeomorphism $f : S \rightarrow T_p$. As S is unknotted this diffeomorphism can be extended to all \mathbb{R}^3 $F : \mathbb{R}^3 \rightarrow \mathbb{R}^3$ such that $F|_S = f$. In this case we construct the surfaces \tilde{I}_1 and \tilde{I}_2 as $\tilde{I}_i = F^{-1}(I_i)$, $i = 1, 2$. They also satisfy the above conditions.

By Theorem 3, we know that for ν sufficiently large there exists $T_\eta^i > 0$ such that $G(t) \subset \{x \in [0, 1]^3 : d(x, I(I_i)) < \frac{\eta}{2}\}$ for all $t > T_\eta^i$, $i = 1, 2$. Then, we choose $T_\eta = \max(T_\eta^1, T_\eta^2)$ and we have

$$G(t) \subset [I(I_1) + B(0, \frac{\eta}{2})] \cap [I(I_2) + B(0, \frac{\eta}{2})], \quad t > T_\eta.$$

Hence $G(t) \subset U_\eta \subset I(S) + B(0, \eta)$ for all $t > T_\eta$. \square

Remark. From the proof above, it is easy to see that if S_1, S_2 are two surfaces for which the condition: “for any $\eta > 0$ there exist some $T_\eta > 0$ such that $G(t) \subset \{x \in [0, 1]^3 : d(x, I(S_i)) < \eta\}$ $i = 1, 2$ for $t > T_\eta$,” is true, then it is also true for $S_1 \cap S_2$.

Using this remark, one can prove that if $S = \{x \in [0, 1]^3 : g(x) = 0\}$ is the knotted surface of Fig. 5, then for any $\eta > 0$ there exist some $T_\eta > 0$ such that

$$G(t) \subset \{x \in [0, 1]^3 : d(x, I(S)) < \eta\} \quad t > T_\eta.$$

For the proof, we consider two unknotted surfaces diffeomorphic to a p -torus such that their intersection is the knotted surface and use the remark above to conclude the proof. How do we construct such surfaces? First of all, observe that by attaching a finite number of thin cylinders (which can be done in a smooth way) we can get a smooth surface diffeomorphic to a p -torus for some $p \in \mathbb{N}$. This can be done in two different ways I_1, I_2 such that the boundary of $I(I_1) \cap I(I_2)$ is diffeomorphic to the knotted surface of Fig. 5 and near to it. Of course such result can be proven for all knotted surfaces where the above strategy can be used. \square

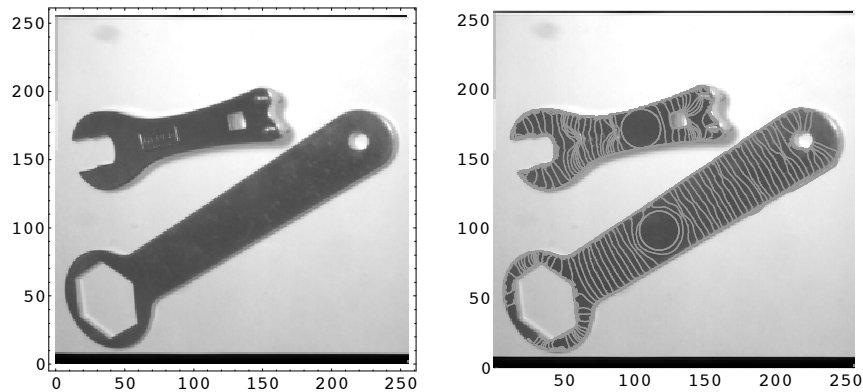


Fig. 4. Example of the geodesic active contours. From the two small circles, both interior and exterior boundaries are detected without any special tracking procedure

Remarks.

1. *Expanding motions.* If $u_0(x)$ is taken as

$$u_0(x) = \begin{cases} > 0 & \text{if } x \in \overline{B(y, r)} \subset I(S) \\ 0 & \text{if } x \text{ in a neighborhood of } S \cup E(S), \end{cases}$$

i.e., a function vanishing in a neighborhood of $S \cup E(S)$, and such that its levels sets have uniformly bounded curvatures, then we may recover a surface S starting from its inner region. The proof of this result is similar to the proof of Theorem 3. Lemma 2 and Lemma 3 are essentially the same except of replacing $I(S)$ by $E(S)$. Hence, we shall omit the details.

2. *Non-ideal edges.* We have shown that the proposed model is consistent for smooth compact surfaces, i.e., when objects hold the basic definition of boundaries ($g \equiv 0$), they are detected by the minimal surfaces approach. As pointed out before, for non ideal edges, previous algorithms [6, 39, 63] will fail, since $g \neq 0$, and the surface will not stop. The new term ∇g creates a potential valley which attracts the surface, forcing the surface to stay there even if $g \neq 0$.
3. *Zero constant velocity.* Similar results can be proved when the constant velocity is equal to zero. In this case, the initial surface should be closer to the final one, to avoid local minima. Again, the existence of the new term ∇g allows also the detection of non convex objects, task which can not be achieved without constant velocity in previous models.

7. Experimental results

We now present some examples of our minimal surfaces deformable model (15). The numerical implementation is based on the algorithm for surface evolution via level sets developed by Osher and Sethian [48, 62] and recently used by many

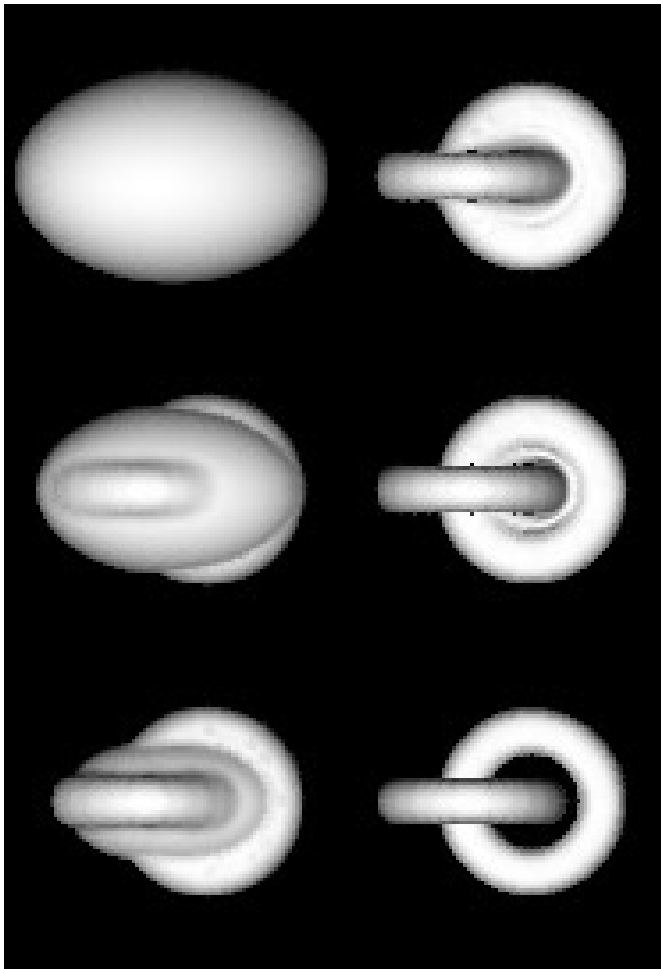


Fig. 5. Detection of two linked tori

authors for different problems in computer vision and image processing. The algorithm allows the evolving surface to change topology without monitoring the deformation. This means that several objects can be detected simultaneously, although it is not required to know that there are more than one in the image. Note that when implementing our model with this algorithm, the extension of the image-based speed performed in [39, 40, 41] is not necessary. Furthermore, using the implementation method introduced in [1], the algorithm can be very efficient (low computational complexity). In the numerical implementation of equation (15) we have chosen central difference approximation in space and forwards difference approximation in time. This simple selection is possible due to the stable nature of the equation, however, when the coefficient ν is taken

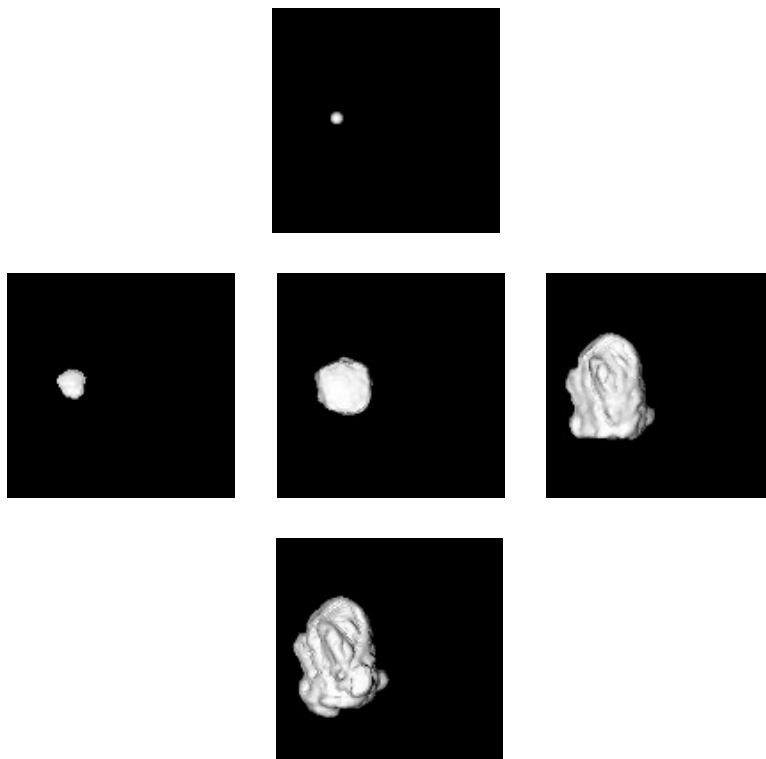


Fig. 6. Detection of a tumor in MRI

to be of high value or when the gradient term is dominant, more sophisticated approximations are required [48].

In our examples, the initialization is in general given by a surface (curve) surrounding all the possible objects in the scene. In the case of outward flows [7], a surface (curve) is initialized inside each object. Multiple initializations are performed in [39, 40, 41, 63]. Although multiple initializations help in many cases, they may lead to false contours in noisy images. Therefore, multiple initializations should in general be controlled (by rough detections of points inside the objects for example) or they should be followed by a validation step.

Figure 4 presents an example of the geodesic active contours taken from [7]. The figure on the left is the original image, and the one on the right present the evolving curves (gray) and the detected boundaries (white). The initial curves are the two small circles in the tools. Both interior and exterior boundaries are detected without any special tracking procedure.

The first example of the minimal surfaces deformable model is presented in Fig. 5. This object is composed of two tori, one inside the other (knotted surface). The initial surface is an ellipsoid surrounding the two tori (top left). Note how the model manages to split and detect this very different topology (bottom right).

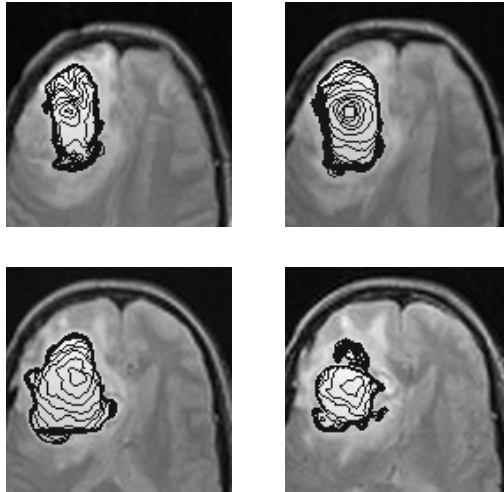


Fig. 7. Slices of the 3D detection in Fig. 6

A medical example is given in Figs. 6 and 7. Figure 6 presents the 3D detection of a tumor in an MRI image. The initial 3D shape is presented in the first row. The second row presents 3 evolution steps, while the final shape, the weighted minimal surface, is presented in the bottom. Figure 7 shows slices of this 3D detection, together with the corresponding MRI data.

8. Concluding remarks

In this paper we presented a novel formulation of deformable surfaces for three dimensional object detection, extending our previously reported two dimensional work [7]. We showed that the solution to the deformable surfaces approach for boundary detection is given by a “minimal surface” in a space derived from the given 3D image. This means that detecting the object is analogue to finding a surface of minimal weighted area. This formulation introduced a new term in previous mean curvature models, improving the attraction of the deforming surface into the boundary. This improves the detection of boundaries with large differences in their gradient. We also presented results regarding the existence, uniqueness, stability, and correctness of the solutions obtained by our model.

We presented experiments for different kind of images. These experiments showed the possibility to detect several objects, as well as the possibility to detect interior and exterior boundaries at the same time. The sub-pixel accuracy intrinsic to the algorithm allows to perform accurate measurements after the object is detected [38, 53].

The model presented is general, as well as the approach for solving image analysis problems via geodesic or minimal surfaces computation. Other image processing and computer vision problems, like the shape from shading [33, 34, 45, 52], can be reformulated as the computation of geodesics or minimal distances

as well. The metric is specified by the image and the application. We are currently investigating this geodesic/minimal-surface-type approach for other problems in image analysis.

Acknowledgements. The authors thank Prof. J. Blat, Prof. P.L. Lions, and Prof. J.M. Morel for interesting discussions and their constant support. The work of RK was supported in part by the Applied Mathematics Subprogram of the Office of Energy Research under DE-AC03-76SFO0098, and ONR grant under N00014-96-1-0381.

References

1. Adalsteinsson, D., Sethian, J.A. (1995): A fast level set method for propagating interfaces. *J. of Comp. Phys.* **118**, 269–277
2. Alvarez, L., Guichard, F., Lions, P.L., Morel, J.M. (1993): Axioms and fundamental equations of image processing. *Arch. Rational Mechanics* **16:IX**, 200–257
3. Alvarez, L., Lions, P.L., Morel, J.M. (1992): Image selective smoothing and edge detection by nonlinear diffusion. *SIAM J. Numer. Anal.* **29**, 845–866
4. Angenent, S. (1991): Parabolic equations for curves on surfaces, Part II. Intersections, blow-up, and generalized solutions. *Annals of Mathematics* **133**, 171–215
5. Blake, A., Zisserman, A. (1987): *Visual Reconstruction*. MIT Press, Cambridge
6. Caselles, V., Catta, F., Coll, T., Dibos, F. (1993): A geometric model for active contours. *Numerische Mathematik* **66**, 1–31
7. Caselles, V., Kimmel, R., Sapiro, G.: Geodesic active contours. *International Journal of Computer Vision* (to appear). (A short version appears at Proc. Int. Conf. Comp. Vision '95, 694–699 Cambridge, June 1995)
8. Caselles, V., Sbert, C. (1996): What is the best causal scale-space for 3D images?. *SIAM J. on Applied Math.* **56:4**, August
9. Chen, Y.G., Giga, A., Goto, S. (1991) Uniqueness and existence of viscosity solutions of generalized mean curvature flow equations. *J. Differential Geometry* **33**, 749–786
10. Chopp, D. (1993): Computing minimal surfaces via level set curvature flows. *J. Computational Physics* **106**, 77–91
11. Cinquin, P. (1986): Un modele pour la representation d'images medicales 3d. *Proc. Euromedicine, Sauramps Medical* **86**, 57–61
12. Cohen, L.D. (1991): On active contour models and balloons. *CVGIP: Image Understanding* **53**, 211–218
13. Cohen, I., Cohen, L.D., Ayache, N. (1992): Using deformable surfaces to segment 3D images and infer differential structure. *CVGIP: Image Understanding* **56**, 242–263
14. Cohen, L.D., Kimmel, R. (1995): Global minimum for active contours models: A minimal path approach. *International Journal of Computer Vision* (to appear). (A short version appeared in Proc. of CVPR'96, pp.666–673, San-Francisco, California)
15. Crandall, M.G., Ishii, H., Lions, P.L. (1992): User's guide to viscosity solutions of second order partial linear differential equations. *Bulletin of the American Math. Society* **27**, 1–67
16. Do Carmo, M.P. (1976): *Differential Geometry of Curves and Surfaces*. Prentice-Hall
17. Dubrovin, B.A., Fomenko, A.T., Novikov, S.P. (1984): *Modern Geometry – Methods and Applications I*. Springer-Verlag, New York
18. Evans, L.C., Spruck, J. (1991): Motion of level sets by mean curvature, I. *J. Differential Geometry* **33**, 635–681
19. Faugeras, O. (1993): On the evolution of simple curves of the real projective plane. *Comptes rendus de l'Acad. des Sciences de Paris* **317**, 565–570, September
20. Faugeras, O. (1993): Cartan's moving frame method and its application on the geometry and evolution of curves in the Euclidean, affine, and projective planes. *INRIA TR* **2053**, September 1993.

21. O. Faugeras and R. Keriven, Scale-spaces and affine curvature. In: Mohr, R., Wu C. (eds.) Proc. Europe-China Workshop on Geometrical Modeling and Invariants for Computer Vision, pp. 17–24
22. Fua, P., Leclerc, Y.G. (1990): Model driven edge detection. *Machine Vision and Applications* **3**, 45–56
23. Gage, M., Hamilton, R.S. (1986): The heat equation shrinking convex plane curves. *J. Differential Geometry* **23**, 69–96
24. Grayson, M. (1987): The heat equation shrinks embedded plane curves to round points. *J. Differential Geometry* **26**, 285–314
25. Guggenheimer, H.W. (1963): *Differential Geometry*. McGraw-Hill Book Company, New York
26. Kass, M., Witkin, A., Terzopoulos, D. (1988): Snakes: Active contour models. *International Journal of Computer Vision* **1**, 321–331
27. Kichenassamy, S., Kumar, A., Olver, P., Tannenbaum, A., Yezzi, A. (1995): Gradient flows and geometric active contour models. Proc. Int. Conf. Comp. Vision '95, 810–815, Cambridge, June
28. Kichenassamy, S., Kumar, A., Olver, P., Tannenbaum, A., Yezzi, A.: Conformal curvature flows: from phase transitions to active vision. *Archive for Rational Mechanics and Analysis* (to appear)
29. Kimia, B.B., Tannenbaum, A., Zucker, S.W. (1990): Toward a computational theory of shape: An overview. *Lecture Notes in Computer Science* **427**, 402–407, Springer-Verlag, New York
30. Kimia, B.B., Tannenbaum, A., Zucker, S.W. (1995): Shapes, shocks, and deformations, I. *International Journal of Computer Vision* **15**, 189–224
31. Kimmel, R., Bruckstein, A.M. (1993): Shape offsets via level sets. *CAD* **25:5**, 154–162
32. Kimmel, R., Amir, A., Bruckstein, A.M. (1995): Finding shortest paths on surfaces using level sets propagation. *IEEE Trans. Pattern Analysis Machine Intelligence* **17**, 635–640
33. Kimmel, R., Bruckstein, A.M. (1995): Tracking level sets by level sets: A method for solving the shape from shading problem. *Computer Vision Image Understanding* **62**, 47–58
34. Kimmel, R., Siddiqi, K., Kimia, B.B., Bruckstein, A.M. (1995): Shape from shading: Level set propagation and viscosity solutions. *International Journal of Computer Vision* **16**, 107–133
35. Kimmel, R., Kiryati, N., Bruckstein, A.M. (1996): Distance maps and weighted distance transforms. Special Issue on Topology and Geometry in Computer Vision *Journal of Mathematical Imaging and Vision* **6**, 223–233, June
36. Kimmel, R., Sapiro, G. (1995): Shortening three dimensional curves via two dimensional flows. *International Journal of Computer & Mathematics with Applications* **29**, 49–62
37. Koller, T., Gerig, G., Szekely, G., Dettwiler, D. (1996): Multiscale detection of curvilinear structures in 2d and 3d image data. Proc. Int. Conf. Comp. Vision '95, pp. 864–869, Cambridge, June
38. Malladi, R., Kimmel, R., Adalsteinsson, D., Sapiro, G., Caselles, V., Sethian, J.A. (1996): A geometric approach to segmentation and analysis of 3D medical images. Proc. Mathematical Methods in Biomedical Image Analysis Workshop, San Francisco, June 21–22
39. Malladi, R., Sethian, J.A., Vemuri, B.C. (1994): Evolutionary fronts for topology independent shape modeling and recovery. Proc. of the 3rd ECCV, Stockholm, Sweden, 3–13
40. Malladi, R., Sethian, J.A., Vemuri, B.C. (1995): Shape modeling with front propagation: A level set approach. *IEEE Trans. Pattern analysis Machine Intelligence* **17:2**, 158–175
41. Malladi, R., Sethian, J.A., Vemuri, B.C.: A fast level set based algorithm for topology independent shape modeling. *Journal of Mathematical Imaging and Vision*, Special Issue on Topology and Geometry, Ed. A. Rosenfeld and Y. Kong (to appear)
42. McInerney, T., Terzopoulos, D. (1995): Topologically adaptable snakes. Proc. Int. Conf. Comp. Vision '95, pp. 840–845, Cambridge, June
43. Mumford, D., Shah, J. (1989): Optimal approximations by piecewise smooth functions and variational problems. *Comm. Pure and App. Math.* **42**
44. Niessen, W.J., ter Haar Romeny, B.M., Florack, L.M.J., Salden, A.H. (1993): Nonlinear diffusion of scalar images using well-posed differential operators. Technical Report, Utrecht University, The Netherlands, October
45. Oliensis, J., Dupuis, P. (1991): Direct Method For Reconstructing Shape From Shading. Proceedings SPIE Conf. 1570 on Geometric Methods in Computer Vision, pp. 116–128
46. Olver, P.J., Sapiro, G., Tannenbaum, A. (1994): Differential invariant signatures and flows in computer vision: A symmetry group approach. In: Romeny, B. (ed.) *Geometry Driven Diffusion in Computer Vision*. Kluwer

47. Olver, P.J., Sapiro, G., Tannenbaum, A.: Invariant geometric evolutions of surfaces and volumetric smoothing. *SIAM J. of Appl. Math.* (to appear)
48. Osher, S.J., Sethian, J.A. (1988): Fronts propagation with curvature dependent speed: Algorithms based on Hamilton-Jacobi formulations. *Journal of Computational Physics* **79**, 12–49
49. Osserman, R. (1986): *Survey of Minimal Surfaces*. Dover
50. Pauwels, E.J., Fiddelaers, P., Van Gool, L.J. (1995): Shape-extraction for curves using geometry-driven diffusion and functional optimization. *Proc. Int. Conf. Comp. Vision '95*, pp.396–401, Cambridge, June
51. Romeny, B. (1994): *Geometry Driven diffusion in Computer Vision*. Kluwer
52. Rouy, E., Tourin, A. (1992): A viscosity solutions approach to shape-from-shading. *SIAM. J. Numer. Analysis* **29**, 867–884
53. Sapiro, G., Kimmel, R., Caselles, V. (1995): Object detection and measurements in medical images via geodesic active contours. *SPIE-Vision Geometry* **2573**, 366–378, San Diego, July
54. Sapiro, G., Kimmel, R., Shaked, D., Kimia, B.B., Bruckstein, A.M. (1993): Implementing continuous-scale morphology via curve evolution. *Pattern Recog.* **26:9**, 1363–1372
55. Sapiro, G., Tannenbaum, A. (1994): On affine plane curve evolution. *Journal of Functional Analysis* **119:1**, 79–120
56. Sapiro, G., Tannenbaum, A. (1993): Affine invariant scale-space. *International Journal of Computer Vision* **11:1**, 25–44
57. Sapiro, G., Tannenbaum, A. (1993): On invariant curve evolution and image analysis. *Indiana University Mathematics Journal* **42:3**
58. Sapiro, G., Tannenbaum, A. (1995): Area and length preserving geometric invariant scale-spaces. *IEEE Trans. Pattern Analysis Machine Intelligence* **17:1**, 67–72
59. Soner, H.M. (1993): Motion of a set by the curvature of its boundary. *J. of Diff. Equations* **101**, 313–372
60. Shah, J. (1995): Recovery of shapes by evolution of zero-crossings. Technical Report, Math. Dept. Northeastern Univ. Boston MA
61. Szeliski, R., Tonnesen, D., Terzopoulos, D. (1993): Modeling surfaces of arbitrary topology with dynamic particles. *Proc. Computer Vision Pattern Recognition*, pp.82–87
62. Sethian, J.A. (1989): A review of recent numerical algorithms for hypersurfaces moving with curvature dependent flows. *J. Differential Geometry* **31**, 131–161
63. Tek, H., Kimia, B.B. (1995): Image segmentation by reaction-diffusion bubbles. *Proc. Int. Conf. Comp. Vision '95*, pp.156–162, Cambridge, June
64. Terzopoulos, D., Witkin, A., Kass, M. (1988): Constraints on deformable models: Recovering 3D shape and nonrigid motions. *Artificial Intelligence* **36**, 91–123
65. Whitaker, R.T. (1994): Volumetric deformable models: Active blobs. *ECRC TR* **94-25**
66. Whitaker, R.T. (1995): Algorithms for implicit deformable models. *Proc. Int. Conf. Comp. Vision '95*, pp.822–827, Cambridge, June
67. Zhu, S.C., Lee, T.S., Yuille, A.L. (1995): Region competition: Unifying snakes, region growing, energy/Bayes/MDL for multi-band image segmentation. *Proc. Int. Conf. Comp. Vision '95*, pp.416–423, Cambridge, June
68. Zucker, S.W., Hummel, R.A. (1981): A three-dimensional edge operator. *IEEE-PAMI* **3**, 324–331

This article was processed by the author using the \LaTeX style file *pljour1m* from Springer-Verlag.